RSC Advances

ROYAL SOCIETY OF CHEMISTRY

www.rsc.org/advances

The Preparation of graphene on nickel film catalyst pre-deposited to fused silica and the corresponding characterization

Xianglian Song [a,b,c], Lixin Song [a,b], Tao Zhang [a,b],*, Xiaoying Chen[a,b]

[a] The Key Laboratory of Inorganic Coating Materials, Chinese Academy of Sciences, 1295 Dingxi Road, Shanghai 200050, PR China

[b] Shanghai Institute of Ceramics, Chinese Academy of Sciences, 1295 Dingxi Road, Shanghai 200050, PR China

[c] University of Chinese Academy of Sciences, 19 Yuquan Road, Beijing 100049, PR China

*Corresponding author: Tel: +86 021-69906175; E-mail address: tzhang@mail.sic.ac.cn; Postal address: 1295 Dingxi Road, Shanghai 200050, PR China.

Abstract: Graphene was prepared with nickel catalyst pre-deposited to fused silica substrate by the chemical vapor deposition (CVD) process including a pre-anneal stage. The critical role of hydrogen in fabricating graphene successfully was confirmed by Raman spectra. Moreover, the purity of the graphene could be improved through adequate pre-anneal by suppressing the formation of graphite nano-rods. After the optimized CVD, it was observed that carbon atoms aggregated into tiny center spots and spread along grain surfaces of the nickel layer, in contrast to the accumulation phenomenon on grain boundaries. Furthermore, characterizations of the multilayer graphene (MLG) adhering directly on fuse silica were carried out, which would reflect the intrinsic properties of MLG grown on nickel film withal.

Keywords: Graphene; Nickel; CVD process; Pre-anneal

1 Introduction

As a two-dimensional allotrope of carbon, graphene has attracted increasing attention since the first announcement in 2004[1]. Owning to its excellent properties in thermodynamic stability, charge-carrier mobility, and

transparency in visible light range[2-5], graphene exhibits promising application in many areas, such as transparent conductive electrodes, field effect transistors, super-conductors, etc. Compared with other common techniques to produce graphene, such as cleavage of graphite[6], decomposition of SiC[7], and reduction of graphene oxide (GO)[8], chemical vapor deposition (CVD)[9,10] has profound advantages in high quality and large scale, which is regarded as one of the most potential methods for practical application[11,12].

In precipitation of graphene through the CVD approach, nickel is a widely used catalyst due to its high carbon solubility and abundant in reserve[13-16]. With nickel assistance, the synthesis of graphene involves at least two basic steps[17,18]. Carbon atoms first dissolute and diffuse into the nickel layer at high temperature, and secondly during the cooling process, segregate and crystallize to form graphene sheets. The segregation of carbon atoms for graphene formation on nickel thin film can be moderated through appropriate annealing treatments in the CVD[19]. It has been demonstrated that a particular pre-anneal stage before growth would provide multiple superiorities in optimizing the nickel film[20,21], which is supposed to be an optimal choose to improve the quality and purity of graphene formulated. However, research investigating the growth of graphene on nickel film through a CVD process with such a pre-anneal stage has rarely been reported.

In our work, the impacts of hydrogen and pre-anneal time on graphene growth were studied at the beginning, so as to ensure the successful formation of high purity graphene on nickel thin film. After the optimized CVD, the segregation behavior of carbon atoms on the whole surface of nickel film were observed, whereas most research before focused mainly on the grain boundaries area[22]. Besides, when the samples were immerged into $FeCl_3$ solution, graphene layers were obtained adhering directly to the surface of fused quartz as nickel layer etched away, which reflected the true state of graphene formulated on nickel surface. Furthermore, The adhering graphene on transparent substrates is of great importance for electrical applications, especially for transparent

conductive electrodes, which is regarded as a promising candidate to replace the widely used indium tin Oxide (ITO)[23]. While, most graphene on transparent substrates are achieved with an extra transfer process, which would bring unexpected defects and reduced performance[24,25].

2 Experimental

Nickel film with a thickness of ~300 nm was deposited onto the fused silica by e-beam evaporation, which was loaded to the left side of a long quartz tube fixed in a sliding furnace CVD system (MTI, OTF-1200X-100SL). The furnace was firstly heated at the right side of the quartz tube to pre-anneal temperature ($T_{pre\text{-}anneal}$). Then as the furnace was moved to the sample area in the left side of the quartz tube, the target samples were heated rapidly to $T_{pre\text{-}anneal}$ in the steady mixture flow of hydrogen (H_2, purity 99.99%) and argon (Ar, purity 99.99%). Later a stabilized pre-anneal stage was carried out at $T_{pre\text{-}anneal}$. Subsequently a growth process was conducted at T_{growth} by introducing the flow of methane (CH_4, purity 99.99%). After growth, methane was shut down, and then the furnace was pulled back to the right side. As a result, samples were rapidly cooled down to room temperature. All the CVD process was conducted under atmosphere pressure. The schematic diagram of the CVD system and the CVD process is illustrated in Fig. 1. According to the gas and temperature statues, the whole CVD process can be roughly divided into three stages in the experiment, as shown in Fig. 1 (b). In stage I, the samples were heated up and kept at $T_{pre\text{-}anneal}$ in the gas mixture of H_2 and Ar. During stage II, CH_4 was introduced as carbon source for subsequent decomposition and growth. In stage III, these samples were cooled rapidly to the room temperature by withdrawing the heating furnace.

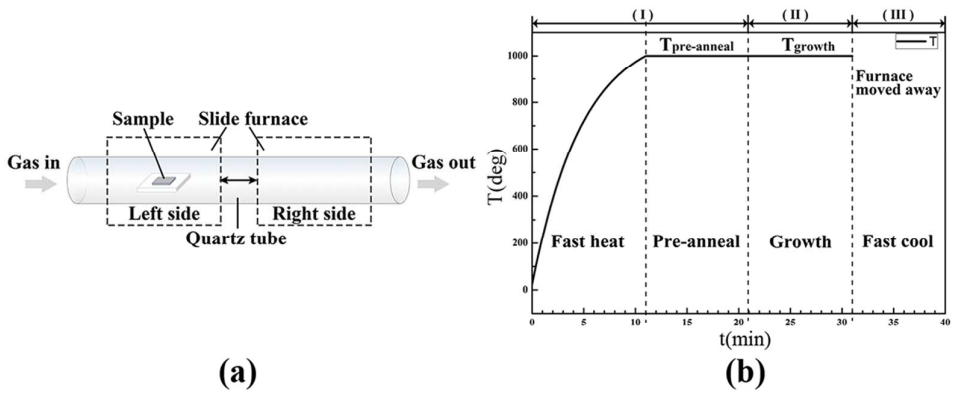

Fig. 1. Schematic diagram of the CVD system (a) and the CVD process (b).

Crystallographic properties of the samples were characterized by X-ray diffraction (XRD). Raman spectra were performed through Renishaw equipment accompanied with a laser excitation at wavelength of 514 nm. Chemical bond information was characterized by X-ray photoelectron spectroscopy (XPS) with a Kratos Axis Ultra spectrometer using a monochromatic Al Kα source. High-resolution scan electron microscope (SEM) images were achieved by Hitachi 8020 facility. The microstructures of graphene sheet were accomplished by high-resolution transmission electron microscope (HRTEM) using Tecnai G2 F20.

3 Results and discussion

3.1 The indispensable role of hydrogen in graphene synthesis

As shown in the XRD spectra in Fig. 2 (a), a strong Ni (111) peak along with a weak Ni (200) can be observed in all the samples treated by CVD processes with different H_2 participation methods, which indicates the formation of dominant Ni (111) grains and a smaller population of Ni (200) grains in the nickel layer. The main Ni (111) orientation provides a perfect match for graphene growth, since the hexagonal lattice space of graphite (2.46 Å) is close to that of Ni (111) (2.497 Å) [26]. Moreover, a characteristic C (002) at 26.3° is recognized, which attributes to be the carbon atoms dissolving in the

nickel layer. The presence of hydrogen in stage II and stage III would accompany with the intensity decline of C (002), corresponding to the concentration decrease of carbon dissolved in the nickel layer as the precipitation occurred at the surface[27].

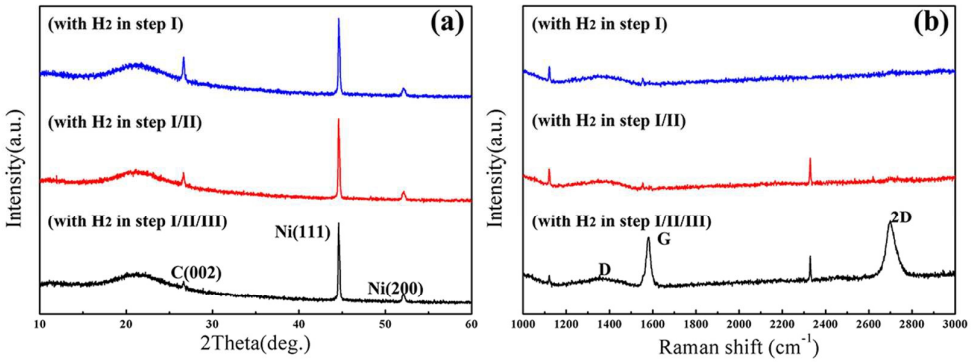

Fig.2. (a) XRD and (b) Raman spectra of samples treated by various hydrogen conditions.

On the other hand, typical Raman spectra were conducted on the samples to confirm the existence of graphene, as illustrated in Fig. 2 (b). The graphene on nickel surface displays characteristic peaks located at ~1350 cm^{-1} (D band), ~1580 cm^{-1} (G band) and ~2700 cm^{-1} (2D band), respectively[11]. The 2D peak, which originates from a double resonance process linking phonons to electronic band structure[28], is normally adopted as a powerful evidence to confirm the existence of graphene. With H_2 participating in step I or in steps I/II, neither typical G nor 2D peak is detected. However, distinctive Raman spectrum of graphene is obtained with H_2 participating in all the three stages. The intensity ratios of D-peak to G-peak ($I_{D/G}$) and 2D-peak to G-peak ($I_{2D/G}$) are 0.49 and 1.22 respectively, which validates the existence of graphene[18]. It should be noted that hydrogen is essential in the whole CVD process, especially in the cooling stage to obtain graphene successfully.

The effect of hydrogen in each stage can be summarized as follows. In stage I, hydrogen would eliminate contaminants and flatten surface, which provide more uniform catalyst surfaces for further graphene formation[20,21]. In stage II, hydrogen would promote the methane absorption and decomposition,

as well as carbon dissolution in the nickel layer[27,29]. Most importantly, hydrogen in the cooling process would assist in carbon segregation on the nickel surface and assure the precipitation of graphene of high quality.

3.2 The suppression of graphite nano-rods impurity

The extra pre-anneal treatment plays an important role in the CVD process to grow graphene of high purity. We investigated the influence of the pre-anneal time while the temperatures for pre-anneal and growth were maintained at 1000℃. However, nano-rods like morphology, namely graphite nano-rods would appear on nickel surface at the same time once the pre-anneal stage is inadequate. As shown in Fig 3(a), two categories of Raman spectra corresponding to multilayer graphene (red color) and graphite nano-rods (blue color) respectively, were acquired simultaneous on samples pre-annealed for 6 min and grown for 10 min at 1000℃. For graphite nano-rods, merging peaks located at 1357 cm^{-1} and 1600 cm^{-1} are detected, which are in regards to the D and G peak[30,31].

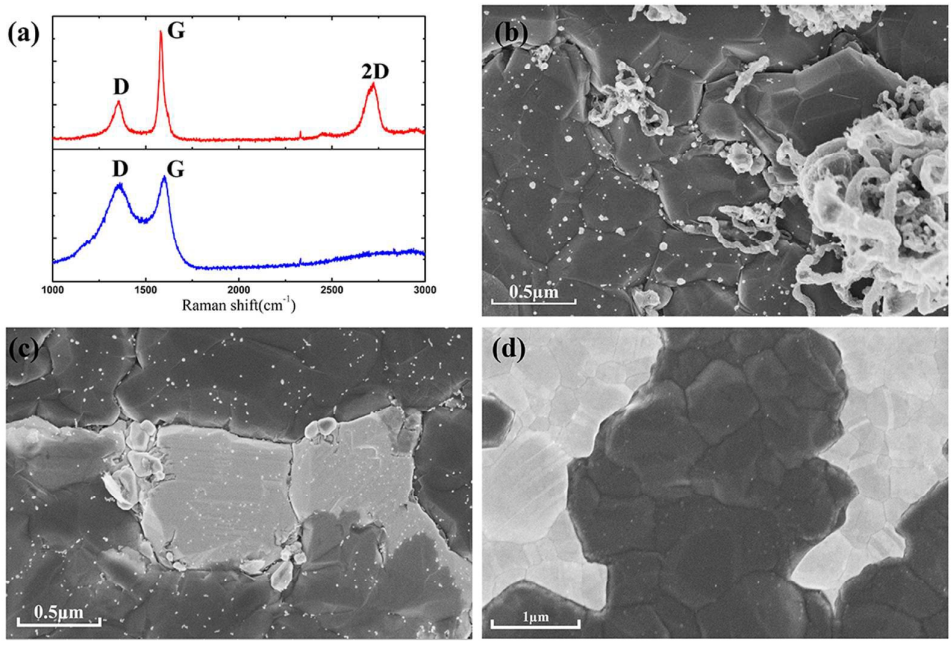

Fig. 3. (a) Raman spectra of the MLG and graphite nano-rods grown on nickel film surface; SEM images of samples (b) pre-annealed for 6 min and grown for 10 min, (c) pre-annealed for 6 min and grown for 6 min, (d) pre-annealed for 10 min and grown for 10 min.

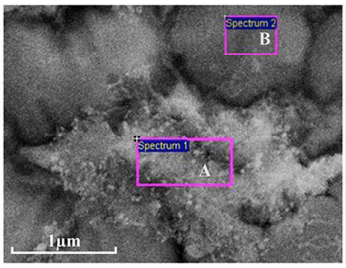

Area	A	B
C K (at.%)	79.00	72.40
Ni K (at.%)	18.62	26.42
O K (at.%)	1.40	0.35
Si K (at.%)	0.98	0.83
Total (at.%)	100	100

Fig. 4. The EDS results evaluated from the areas with (A) and without (B) graphite nano-rods on nickel film pre-annealed for 6 min and grown for 10 min.

As the SEM image shown in Fig. 3 (b), the nickel film pre-annealed for 6 minutes and grown for 10 minutes at 1000 ℃ is covered with graphite nano-rods clusters. Long rods gathering around the grain boundaries and particles of different sized on the grain surface are found on the nickel film. The growth of the graphite nano-rods can be further observed by decreasing the growth time to 6 minutes, as shown in Fig. 3 (c). Anomalous granules distribute along the grain-boundaries, and numerous much smaller tiny spots spread over the grain surfaces at the early stage. Nevertheless, none graphite nano-rod can be found on nickel surface any more as the pre-anneal time increases to 10 minutes, as shown in Fig. 3 (d). Additionally, energy dispersive spectrometer (EDS) analyses are carried out to verify the nature of nano-rod cluster, indicating that the cluster (A) has a higher percentage of carbon, and a corresponding lower percentage of nickel than the other area (B), as shown in Fig. 4. It is concluded that the increase of pre-anneal time effectively prevent the unpredicted growth of graphite nano-rods on the nickel film surface.

3.3 The segregation of carbon atoms on the nickel film surfaces

After the optimized CVD process, the segregation of carbon atoms on the nickel film surface is clearly obvious, which would meanwhile clarify the precipitation phenomenon. As shown in Fig. 5, graphene is obtained on the surface of nickel film, and the darker contrasts are responsible for multilayer graphene layers[32]. It can be observed in Fig. 5 (a) that carbon atoms accumulate along grain-boundaries, relating

closely to the high curvature and thus high density of atomic steps at the boundaries[20,21]. Furthermore, for the grain surfaces of nickel film, darker contrasts can be found around the tiny spots (Fig. 5 (b)). The segregation of carbon on the grain surfaces of nickel film is supposed to start from tiny center spots outward, with spreading steps obviously observed in Fig. 5 (c). These spots on the grain surfaces could "pump" carbon atoms out of nickel layer, spread them along surface profile, and form multilayer graphene near the center and formulate single/bilayer at a distance. As a result, multiple-layers and single/bilayer graphene are recognized on the nickel film. Besides, visible twinkles could be observed connecting with active spots in Fig. 5 (b), which are related to the stress release arising from the deviation of thermal expansion coefficients between the nickel and graphene[34].

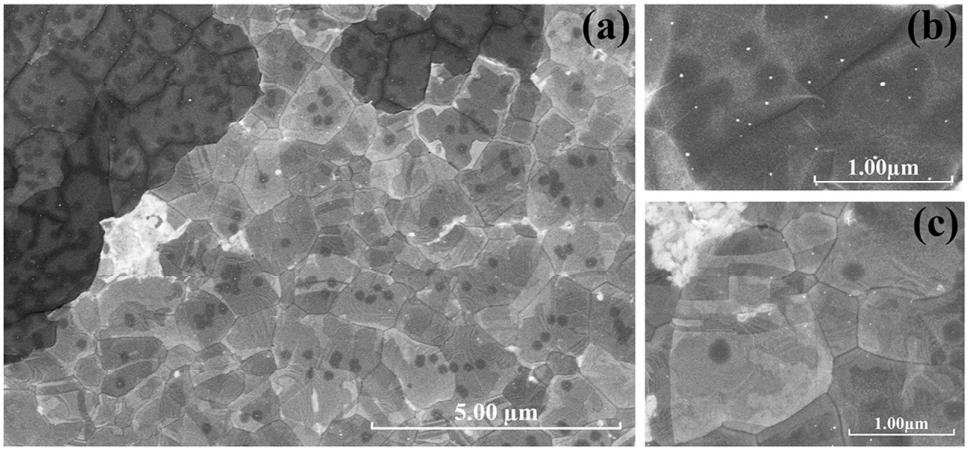

Fig. 5. (a) Morphological characterizations of carbon atoms segregating on nickel film surface, (b) and (c) high resolution SEM images of the grain boundaries area and grain surfaces of nickel catalyst after the CVD process.

3.4 Graphene attaching directly to fused silica after etching

The segregation of carbon atoms to form MLG on the surface of nickel thin film is obvious, and the multilayer graphene would adhere directly onto substrate surface when immerging in ferric chloride ($FeCl_3$) solution with a concentration of 0.1 mol/L, as confirmed by Raman spectrum (Fig. 6 (a)). From the position and shape of Raman peaks, it could be drawn that multilayer and monolayer/bilayer graphene existed at the same time on surface of fuse quartz. The 2D peak of multilayer graphene is much

lower than the G peak, with a minor shift to the higher energy[28]. What's more, the 2D peak of the monolayer/bilayer graphene has a single Lorentzian profile, and the intensity ratio of the 2D-peak and G-peak is higher than 1[20]. Because of the phonon scattering in the lattice defects[12], a small band at the position of ~1608 cm^{-1} can be also recognized. Extra identification about the chemical state is carried out by XPS on the film surface, as shown in Fig. 6 (b). A dominant peak located at ~284.8 eV originating from the C-C sp^2 bonding[33] is recognized, verifying the existence of graphene on surface of fuse silica.

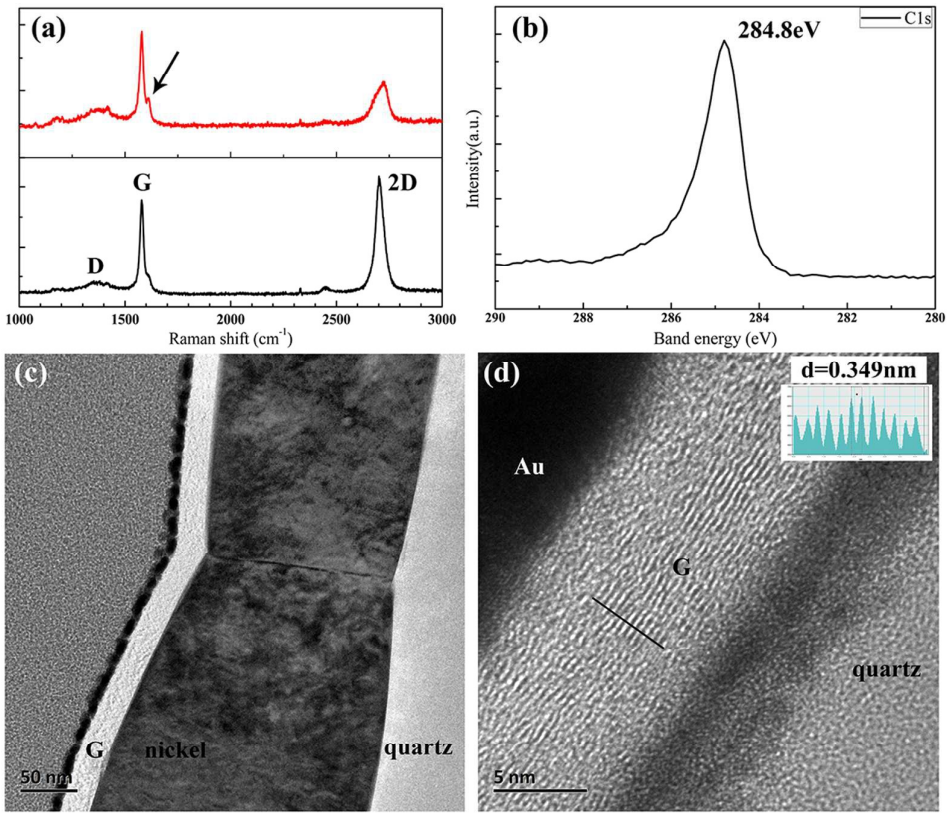

Fig.6. (a) Raman spectra and (b) XPS result of C^{1s} peak (b) of the MLG on fuse silica after $FeCl_3$ etching. Cross-sectional TEM images of MLG formulated on (c) nickel film (before etching) and on (d) fused silica (after etching) respectively.

TEM specimens of the MLG grown on nickel surface and MLG adhering to fused silica were fabricated by the focus ion beam (FIB) technology for straightly cross observation. As shown in Fig.6 (c), before etching, multilayer graphene has been

grown on the nickel film surface, whereas none graphene sheet can be observed at the interface between nickel and fused quartz. The results indicate that the segregation of carbon atoms is easier on the top surface of nickel layers than the interface. However, multilayer graphene would show on the fused silica surface after the etching treatment of $FeCl_3$ solution, as the TEM image shown in Fig. 6 (d). The distance between layers is measured to be 0.349 nm, as the inset image displayed in Fig. 6 (d). Moreover, the discontinuous points exist in the multilayer graphene on fused quartz at the same time, which coincides with the D-band detected in the Raman spectrum.

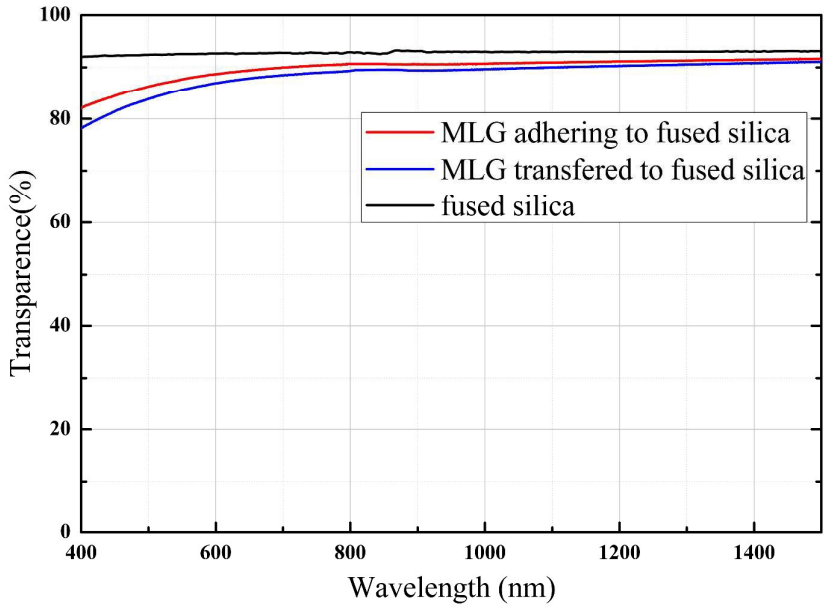

Fig.7. Optical Transparence of MLG obtained by adhesion and transfer with blank fused silica.

In Fig. 7, the transparency (400nm to 1500 nm) of multilayer graphene adhering directly to fused silica is compared with blank fuse silica, and with multilayer graphene obtained through conventional transferring process[16] with PMMA assistance. It can be observed that the transparence of MLG adhering directly to quartz is higher than that from transferring, for which the transmittance is ~90% from 700~1500 nm wavelength. Moreover, the sheet resistance of MLG (0.9~1.2KΩ/sq) adhering directly to fused silica is much lower than the transferred film (2.2~2.6$K\Omega/sq$), which is acquired from the four-probe measurement. In fact, the MLG acquired from the two

methods both originates from the nickel film surface, which is supposed to have similar properties. The properties of MLG obtained from direct adhering have a better coincidence with that obtained on nickel surface, which would offer better instruction to promote the practical application of graphene.

Conclusion

In summary, we have adopted an optimized thermal CVD process including an extra pre-anneal process to synthesis graphene with nickel catalyst pre-deposited to fused silica. It is established that hydrogen plays an essential role in promoting the formation of graphene, especially in the cooling stage. Moreover, the purity of formulated graphene can also be improved with subsequent pre-anneal time. The optimized CVD contributes to the segregation of carbon atoms on nickel film, which further illustrates the formation mechanism of graphene, and provides a new insight for the direct growth of graphene on transparent dielectric substrates.

References

[1] K.S. Novoselov, A.K. Geim, S.V. Morozov, D. Jiang, Y. Zhang, S.V. Dubonos, I.V. Grigorieva, A.A. Science, 2004, **306**, 666-669.

[2] J.C. Meyer, A.K. Geim, M.I. Katsnelson, K.S. Novoselov, T.J. Booth, and S. Roth, Nature, 2007, **446**, 60-63.

[3] K.S. Novoselov, A.K. Geim, Nat. Mater, 2007, **6**, 183-197.

[4] A.V. Tyurnina, K. Tsukagoshi, H. Hiura, A.N. Obraztsov, Carbon, 2013, **52**, 49–55.

[5] R.S. Edwards, K.S. Coleman, Nanoscale, 2012, **5**, 1-13.

[6] L. Zhang, X. Li, Y. Huang, Y. Ma, X. Wan, Y. Chen, Carbon, 2010, **48**, 2367-2371.

[7] P. Lauffer, K.V. Emtsev, R. Graupner, T. Seyller, L. Ley, S.A. Reshanov, Phys. Rev. B, 2008, **77**, 155426.

[8] H. Tanaka, S. Obata, K. Saiki, Carbon, 2013, **59**, 472-478.

[9] A. Reina, X. Jia, J. Ho, D. Nezich, H. Son, V. Bulovic, Nano Lett, 2009, **9**, 30-35.

[10] N. Campos, A.M. Perez-Mas, P. Alvarez, R. Menendez, D. Gomez, App. Surf. Sci, 2015, **349**, 101-107.

[11] S. Bae, H. Kim, Y. Lee, X. Xu, J.S. Park, Y. Zheng, Nat. Nanotechnol, 2010, **5**, 574-578.

[12] G. Nandamuri, S. Roumimov, R. Solanki, Nanotechnology, 2010, **21**, 145604.

[13] Z. Fogarassy, M.H. Rummeli, S. Gorantla, A. Bachmatiuk, G. Dobrik, K. Kamaras, L.P. Biro, K. Havancsak, J.L. Labar, App.Surf. Sci, 2015, **314**, 490-499.

[14] R.S. Edwards, K.S. Coleman, Accounts. Chem. Res, 2013, **46**, 23-30.

[15] C.Y. Chen, D. Dai, G.X. Chen, J.H. Yu, K. Nishimura, C.T. Lin, N. Jiang, Z.L. Zhan, App. Surf. Sci, 2015, **346**, 41-45.

[16] X. Li, W. Cai, L. Colombo, R.S. Ruoff, Nano. Lett, 2009, **9**, 4268-4272.

[17] A. Dahal, M. Batzill, Nanoscale, 2014, **6**, 2548-2562.

[18] Q. Yu, J. Lian, S. Siriponglert, H. Li, Y.P. Chen, S.S. Pei, Appl. Phys. Lett, 2008, **93**, 113103.

[19] Q.Yu, J. Lian, S. Siriponglert. H. Li, Y. Chen; S. Pei, Appl. Phys. Lett, 2008, **93**, 113103.

[20] Y. Zhang, T. Gao, S. Xie, B. Dai, L. Fu, Y. Gao, Nano. Res, 2012, **5**, 402-411.

[21] Y. Zhang, L. Gomez, F.N. Ishikawa, A. Madaria, K. Ryu, C. Wang, J. Phys. Chem. Lett, 2010, **1**, 3101-3107.

[22] C. Lu, C. Jin, Y. Lin, C. Huang, K. Suenage, P. Chiu, Langmuir, 2011, **27**, 13748-13753.

[23] Y. Yi, L. Song, X. Song, T. Zhang, J. Alloy. Compd. 2013, **281**, 133-138.

[24] L. G. De Arco, Y. Zhang, C.W. Schlenker, K. Ryu, M. E. Thompson, and C. Zhou, ACS Nano, 2010, **4**, 2865-2873.

[25] Y. Lee, S. Bae, H. Jang, S. Jand, S. E. Zhu, S. H. Sim, Y. I. Song, B. H. Hong, and J. H. Ahn, Nano Lett, 2010, **10**, 490-493.

[26] S. Thiele, A. Reina, P. Healey, J. Kedzierski, P. Wyatt, P.L. Hsu, Nanotechnology, 2010, **21**, 015601.

[27] M. Losurdo, M.M. Giangregorio, P. Capezzuto, G. Bruno, Phys. Chem. Chem. Phys, 2011,**13**, 20836-20843.

[28] A.C. Ferrari, J.C. Meyer, V. Scardaci, C. Casiraghi, M. Lazzeri, S. Piscanec, D.Jiang, K.S. Novoselv, S. Roth, A.K. Geim, Phys. Rev. Lett, 2006, **97**, 187401.

[29] L. Baraton, Z.B. He, C.S. Lee, C.S. Cojocaru, M. Châtelet, J.L. Maurice, Europhys Lett, 2011, **96**, 46003.

[30] W. Yen, Y. Chen, C. Yeh, J. He, P. Chiu, Y. Chueh, Scientific Reports, 2014, **4**, 4739.

[31] T. Takami, R. Seino, K. Yamazaki, T. Ogino, J. Phys. D: Appl. Phys, 2014, **47**, 094015.

[32] Y. Lee, J.H. Ahn, J. Appl. Phys, 2013, **113**, 194305.

[30] R. Zhang, Z.S. Wang, Z.D. Zhang, Z.G. Dai, L.L. Wang, H. Li, Appl. Phys. Lett, 2013, **102**, 193102.

[33] A.N. Obraztsov, E.A. Obraztsova, A.V. Tyurnina, A.A. Zolotukhin, Carbon, 2007, **45**, 2017-2021.

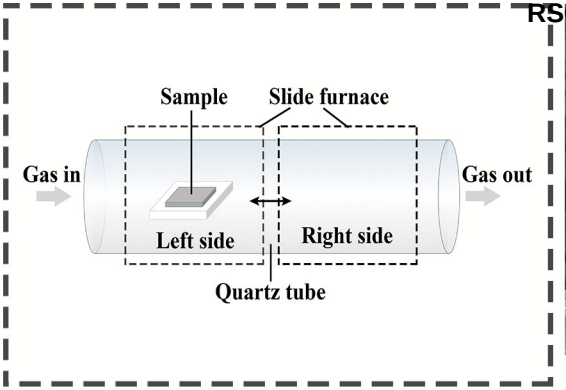

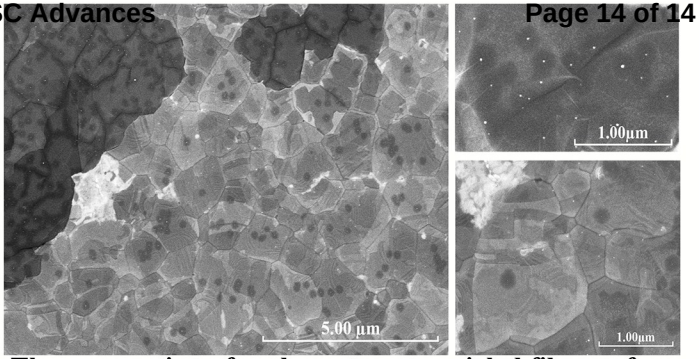

The segregation of carbon atoms on nickel film surface